Tailoring the resonance wavelength and loss of highly Ga doped ZnO plasmonic materials by varied doping content and substrate temperature

Chaoting Zhu [a], Jia Li [a], Ye Yang [a,*], Pinjun Lan [a], Jinhua Huang [a], Yuehui Lu [a], Ruiqin Tan [b], Ning Dai [c], Weijie Song [a,d,**]

[a] Ningbo Institute of Material Technology and Engineering, Chinese Academy of Sciences, Ningbo 315201, PR China
[b] College of Information Science and Engineering, Ningbo University, Ningbo 315201, PR China
[c] National Laboratory for Infrared Physics, Shanghai Institute of Technical Physics, Chinese Academy of Sciences, Shanghai 200083, PR China
[d] Ningbo Key Laboratory of Silicon and Organic Thin Film Optoelectronic Technologies, Ningbo 315201, PR China

A B S T R A C T

In this paper, Ga-doped ZnO (GZO) thin films are deposited on glass substrates by radio frequency magnetron sputtering for low loss plasmonic applications. The effects of Ga_2O_3 content in the target and substrate temperature on the electrical, structural and optical properties of GZO films are investigated. Film with the highest carrier concentration of 7.0×10^{20} cm^{-3} was obtained at a Ga_2O_3 content of 5 wt% in the target under room temperature deposition. With increasing deposition temperature, the lowest electrical resistivity of 3.8×10^{-4} Ω cm was acquired at a deposition temperature of 200 °C. The values of plasmonic resonances wavelength could be changed from 1.35 to 2.39 μm by adjusting the carrier concentration. Material absorption losses in these GZO films are 10 times lower than that of conventional Ag films at telecommunication wavelengths. These results make GZO a promising low-loss plasmonic material operating at telecommunication wavelengths.

Keywords:
Doped zinc oxide
Gallium doping
Plasmonic materials
Magnetron sputtering
Thin films

1. Introduction

The emergence of plasmonic metamaterials opens a new perspective to improve the speed of information processing [1–4]. Metal-based plasmonic materials offer higher speed of information processing than silica fibers at standard operational wavelength [5–7]. Unfortunately, the typical carrier concentrations in metals are too high to push the plasmonic resonance wavelength (λ_{res}) to the near-infrared (NIR) spectral range [8–10]. Additionally, metals also suffer from high optical losses at telecommunication wavelength arising in part from intra-band electronic transitions [11–13]. Hence, there is still an urgent requirement in searching better material building blocks to improve the speed of information processing at telecommunication wavelengths.

Recently, the heavily doped semiconductors have been found to exhibit a moderate plasmonic resonance wavelength and a low loss in the mid-infrared and NIR [14–17]. Among these heavily doped semiconductors, Ga doped ZnO (GZO) transparent conducting oxide is a good candidate as plasmonic materials in the NIR due to its high solid solubility and doping efficiency without severe lattice distortion [16–21]. Moreover, GZO is considered to be more potential to achieve an appropriate concentration to support collective oscillations of free electrons at telecommunication wavelengths [22,23].

Several techniques have been reported in the literature to deposit GZO thin films including pulsed laser deposition [24], chemical vapor deposition [25], atomic layer deposition [26], and radio-frequency magnetron sputtering (RFMS) [27]. Among these deposition techniques, RFMS is quite simple and widely used in industry. In addition, it is possible to produce highly conductive and transparent GZO thin film without heating the substrate, due to the additional energy delivered from the plasma [28].

For the RFMS deposited GZO thin films, the basic fabrication conditions including Ga_2O_3 doping concentration in GZO ceramic target and MS substrate temperature are the key parameters to affect the film electrical properties, such as carrier concentration, which directly changes the plasmonic resonance wavelength according to the Drude theory [29–36]. Therefore, the adjustment on these basic parameters is necessary to optimize the carrier concentration of GZO film and ensure moderate plasmonic resonance wavelength suitable for plasmonic applications in the NIR. Several studies have been reported about the influence of fabrication parameters on the electrical and optical properties of GZO thin films [28–34]. However, most of these research results do not involve plasmonic resonances wavelength and absorption losses of GZO thin films. Recently, D.C. Look et al. demonstrated that plasmonic resonances wavelength of 1.3 and 1.55 μm in GZO films could be accurately adjusted

* Corresponding author.
** Correspondence to: W. Song, Ningbo Institute of Material Technology and Engineering, Chinese Academy of Sciences, Ningbo 315201, PR China.
E-mail addresses: yangye@nimte.ac.cn (Y. Yang), weijiesong@nimte.ac.cn (W. Song).

by post-annealing in air [8]. J. Kim et al. also reported that plasmonic resonances wavelength of GZO films could be changed by doping concentrations of 2, 4, 6 wt% and thermal annealing temperatures [35]. Our recent results also showed that plasmonic resonances wavelength in GZO films could be regulated by the inserted Zn layer thickness [36].

Although some methods on regulating plasma resonance wavelength have been reported, it is important to systematically study the effect of doping concentration in the target and substrate temperature on the plasmonic resonance wavelength and absorption losses of GZO films in the NIR range. In this paper, we deposited GZO thin films by RFMS on glass substrate. The effects of the Ga_2O_3 content in the target and substrate temperature on the electrical, structural and optical properties of GZO thin films are investigated in detail for the plasmonic material applications at telecommunication wavelengths.

2. Experiment

GZO thin films with a thickness of ~500 nm were deposited on soda-lime glass substrates by a RFMS apparatus. The GZO targets were the home-made 3-in. ceramic disks. The Ga_2O_3 contents in GZO targets were 2 wt%, 3 wt%, 4 wt%, 5 wt%, and 6 wt%, respectively. Prior to deposition, the glass substrates were ultrasonically cleaned in deionized water, followed by acetone solution and alcohol, and then dried in nitrogen. The substrates were placed inside the sputtering chamber and then evacuated to a base pressure of 5×10^{-4} Pa. In order to improve the uniformity of the GZO films, the sample holder rotated at a constant speed of 10 rpm/min.

During deposition, RF power was set at 200 W, Ar gas flow rate was fixed at 30 sccm which was controlled by the mass flow controller, work pressure was set at 0.45 Pa and the deposition time was 30 min. Besides, the substrate temperatures were set at room temperature (unintentional heating), 150 °C, 200 °C, 250 °C and 300 °C, respectively.

The crystalline phase of the films was analyzed by X-ray diffraction (XRD, Bruker, AXS D8 Advance, USA) using a standard θ–2θ geometry diffractometer with Cu Kα radiation(λ = 1.54 Å). Morphology of the GZO films was observed by a field emission scanning electron microscopy (FESEM, S4800) at an operating voltage of 4 keV. The resistivity, Hall mobility and carrier concentration of the films were analyzed by Hall measurement with the Van der Pauw method (Accent, HL5500PC, UK). The thickness of the coated GZO films was measured by an M-2000DI Ellipsometry (J. A. Woollam) according to the Cauchy model. The complex refractive index and dielectric constants of the films were determined by fitting a Drude + Lorentz oscillator model [35] to the ellipsometry data. The fitting spectral region ranges from 190 nm to 1750 nm. The resonance energy of the Lorentz oscillator is set to 3.7 eV in correspondence to the interband absorption. The amplitude and damping constants of Lorentz oscillator and Drude term and the permittivity ε_∞ are fit parameters. The optical transmittance and reflection spectrum was obtained by ultraviolet–visible-NIR spectrophotometer (PerkinElmer, LAMBDA950). The absorption spectrum was calculated by the formula: Absorption + Transmission + Reflection = 100%. The measuring spectral region ranges from 250 nm to 2500 nm.

3. Results and discussion

3.1. Electrical properties

The electrical properties of the GZO thin films intensively depend on the fabrication parameters of Ga_2O_3 content in the target and substrate temperature [37–40]. Fig. 1a shows the variation of resistivity (ρ), carrier density (n), and Hall mobility (μ) as a function of Ga_2O_3 content (Ng) in the target for GZO films grown at room temperature (RT). The lower resistivity GZO films ($5 \sim 6 \times 10^{-4}$ Ω cm) can be obtained at Ng from 4 to 6 wt%. It can be attributed to the substitution of Ga elements into Zn site [39], since the Ga_{Zn} defects are the main donor defects contributing to the enhancement of *n*-type conductive [41]. As the Ng increased from 2 wt% to 5 wt%, the correspondingly increased donor defects lead to an enhancement of carrier concentration and a decrease in resistivity. The highest carrier concentration reached 7×10^{20} cm^{-3} for the film with a Ng of 5 wt%, and then slightly decreased to 6.4×10^{20} cm^{-3} at Ng of 6 wt%. It can be deduced that Ga has a higher doping efficiency and solid solubility in ZnO system, and the optimized Ng is 5 wt%. Fig. 1b shows the electrical properties of GZO films with Ng of 5 wt% in the target as a function of substrate deposition temperature (Ts). As the Ts increased from RT to 200 °C, the resistivity decreased from 5.5×10^{-4} to a minimum value of 3.7×10^{-4} Ω cm. This decrease originates from the increased carrier mobility, which can be attributed to an increase in the grain size of the GZO film with increasing Ts to reduce the grain boundary scattering [38,40]. As Ts is further increased from 200 to 300 °C, an increase in the resistivity is observed as a combination of a decrease in carrier density from 6.87×10^{20} to 4.09×10^{20} cm^{-3} and a slight increase in the Hall mobility from 25.2 to 28.3 cm^2V^{-1} s^{-1}. The segregation of Ga_2O_3 at the grain boundaries in the films is responsible for the increase of resistivity when substrate temperature exceeds 200 °C [42]. Hence, the GZO film with highest carrier concentration can be obtained at Ng of 5 wt% and Ts of RT.

3.2. Structural properties

To investigate the crystalline structural properties of GZO films, X-ray diffraction measurement is employed and shown in Fig. 2. All the films exhibit preferential growth with a strong diffraction peak at 2θ = ~34.4°, which is originated from ZnO (002) planes (JCPDS No. 36-1451), indicating typical hexagonal wurtzite structure with c-axis preferred orientation. Fig. 2a shows the XRD patterns of GZO films

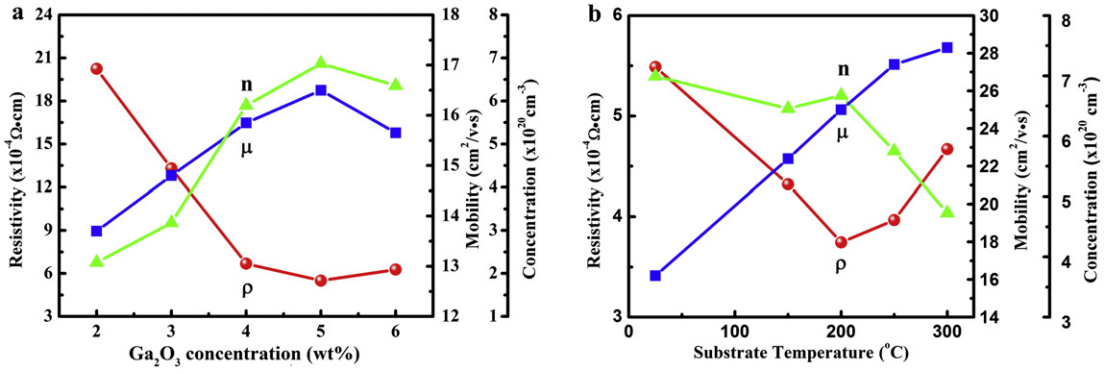

Fig. 1. Resistivity (ρ), carrier density (n), and Hall mobility (μ) of GZO films grown (a) at RT using the sputtering targets with various Ga_2O_3 doping contents (2, 3, 4, 5 and 6 wt%), and (b) at various substrate temperatures (RT, 150, 200, 250 and 300 °C) using the sputtering target with a Ga_2O_3 doping content of 5 wt%. The film thickness was ~500 nm.

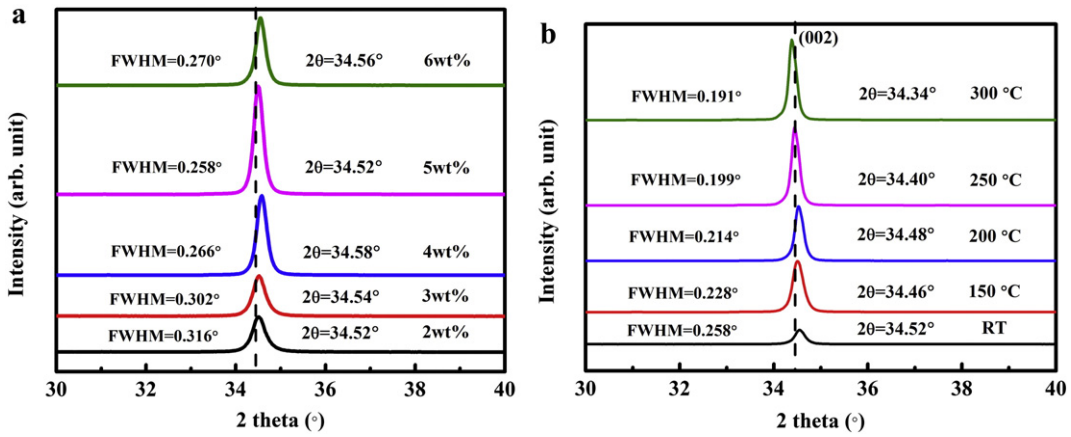

Fig. 2. XRD patterns of GZO films grown (a) at RT using the sputtering targets with various Ga_2O_3 doping contents (2, 3, 4, 5 and 6 wt%), and (b) at various substrate temperatures (RT, 150, 200, 250 and 300 °C) using the sputtering target with a Ga_2O_3 doping content of 5 wt%.

deposited at RT with different Ng. As the Ng increases from 2 wt% to 4 wt%, the (002) 2θ diffraction angles move from 34.52° to 34.58°. Noting that the radius of Ga^{3+} ion (0.62 Å) is smaller than that of Zn^{2+} ion (0.72 Å), the substitution of Ga^{3+} to Zn^{2+} leads to the decrease of the c-axis lattice parameter. Based on Bragg diffraction formula, the decrease of c-axis lattice parameter results in the increase of (002) diffraction angles. As the Ng is further increased from 4 wt% to 5 wt%, the position of (002) peak declines slightly. It may be due to the existence of gallium interstitial (Ga_i) [43]. When the Ng reaches 6 wt%, the position of (002) peak increases slightly due to the existence of small amount of Ga_2O_3 derived from limited solid solubility and doping efficiency. Fig. 2b shows the XRD patterns of GZO films with Ng of 5 wt% deposited at different Ts. It can be seen that the intensities of (002) peaks obviously increase as the Ts increasing from RT to 300 °C. It means that the crystalline quality of the samples has an obvious improvement, furthermore enhancing the Hall mobility. As the Ts increases, the position of (002) peaks shift to lower 2θ values, indicating that the c-axis lattice parameter increases with growth temperature. It could be explained by the decrease of the number of substitutional Ga^{3+} ions into Zn^{2+} sites as increasing TS, especially at the temperature higher than 200 °C [39]. The grain size can be calculated from the full width at half maximum of the (002) diffraction peak by using the Scherrer formula [44], and the corresponding grain sizes of all films are in the range of 35 to 51 nm.

Fig. 3 shows the surface and cross-sectional view of SEM micrographs deposited at various Ng and Ts. Fig. 3a–e shows the surface

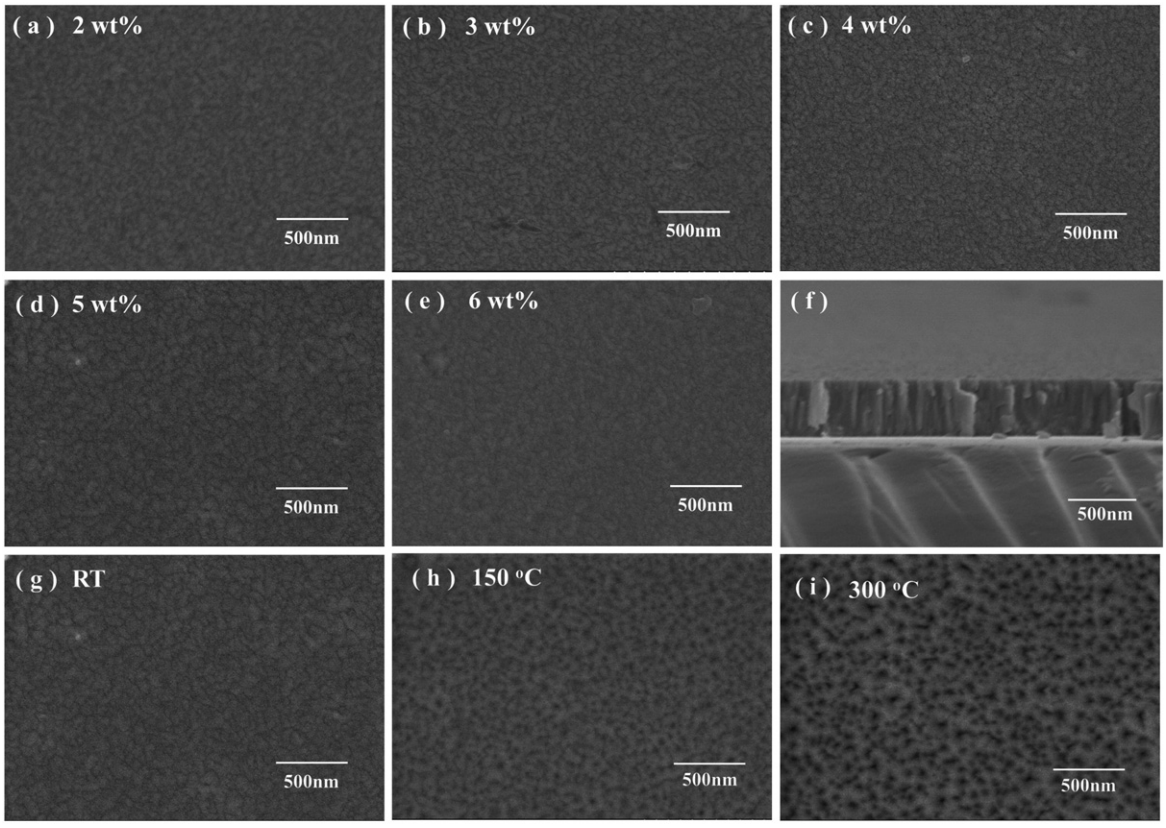

Fig. 3. Surface morphologies of GZO thin films. (a) 2 wt% (RT), (b) 3 wt% (RT), (c) 4 wt% (RT), (d) 5 wt% (RT), (e) 6 wt% (RT), (g) 5 wt% (RT), (h) 5 wt% (150 °C), (i) 5 wt% (300 °C). Cross section of GZO film deposited at RT. (f) 5 wt% (RT).The scale bar is 500 nm.

micrographs of GZO thin films deposited at various Ng. There is no obvious variation except the average size of grains. Fig. 3g–i shows the surface micrographs of GZO thin films deposited at various Ts. The surface of GZO thin films deposited at RT is extremely uniform. Nevertheless, GZO thin film grown above 150 °C shows a rougher surface morphology with many small pits. The substituted Ga atoms in ZnO affect the growth behavior of thin films. The cross sectional view of 5 wt% GZO film deposited at RT is shown in Fig. 3f. The high compact structure shows a typically dense columnar growth, as shown in literature [38].

3.3. Optical properties

The optical transmittances as a function of the wavelength for the GZO films deposited at different Ng and Ts are shown in Fig. 4a and c, respectively. The average transmittances of all films are above 85% in the wavelength range of 400–800 nm. The near-infrared transmittances decrease with the increase of Ng (Fig. 4a) and the decrease of Ts (Fig. 4c). These changes of the optical properties originated directly from the increase of the carrier concentration, which leads to a lower value associated to the plasma wavelength [45]. Fig. 4b and d shows absorption spectra for the GZO films deposited at different Ng and Ts, respectively. Due to the plasma oscillation, the maximum absorption peak occurs at the characteristic plasma wavelength, λ_p [46]. As the Ts decreases, λ_p shifts to shorter wavelengths, which can be attributed to the change of carrier concentration [8].

Fig. 5 shows the variation of n, measured λ_p and calculated λ_p as a function of Ng and Ts for the GZO films. Both of the λ_p are inversely related to n in the GZO films. This behavior can be expressed by the equation: $\lambda_P = \sqrt{\frac{4^2 c^2 m^* \varepsilon_0 \varepsilon_\infty}{Ne^2}}$

where c is the speed of light in a vacuum, ε_∞ is the high-frequency dielectric constant, ε_0 is the permittivity of free space, m^* is the effective mass of electrons, N is the carrier concentration and e is the electron charge. Taking ε_∞ at infinity as 4 and m^* as 0.3 [42], N is obtained from the Hall measurements, calculated λ_p can be estimated from the equation above. The estimated λ_p in Fig. 5a is in the range of 1384–2413 nm for samples with various Ng. The estimated λ_p in Fig. 5b is in the range of 1384–1630 nm for samples with different Ts. The measured λ_p can be obtained from the maximum absorption peak in Fig. 4b and d, where λ_p are found to range from 1375 to 2385 nm and 1375 to 1630 nm, respectively. It is obviously found that these measured data are in good agreement with the calculated data. Thus, the plasmonic resonance wavelength for GZO films can be accurately tuned by varying the carrier density introduced by the Ng and Ts.

To demonstrate the GZO thin films as an alternative plasmonic metamaterials, we obtained the complex refractive indexes and dielectric constants of the films by fitting a Drude + Lorentz oscillator model [35] to the ellipsometry data. The following equation describes the Drude–Lorentz oscillator model.

$$\varepsilon_{(\omega)} = \varepsilon_\infty - \frac{\omega_p^2}{\omega(\omega + i\Gamma_p)} + \frac{f_l \omega_1^2}{\omega_l^2 - \omega^2 - i\omega\Gamma_l}$$

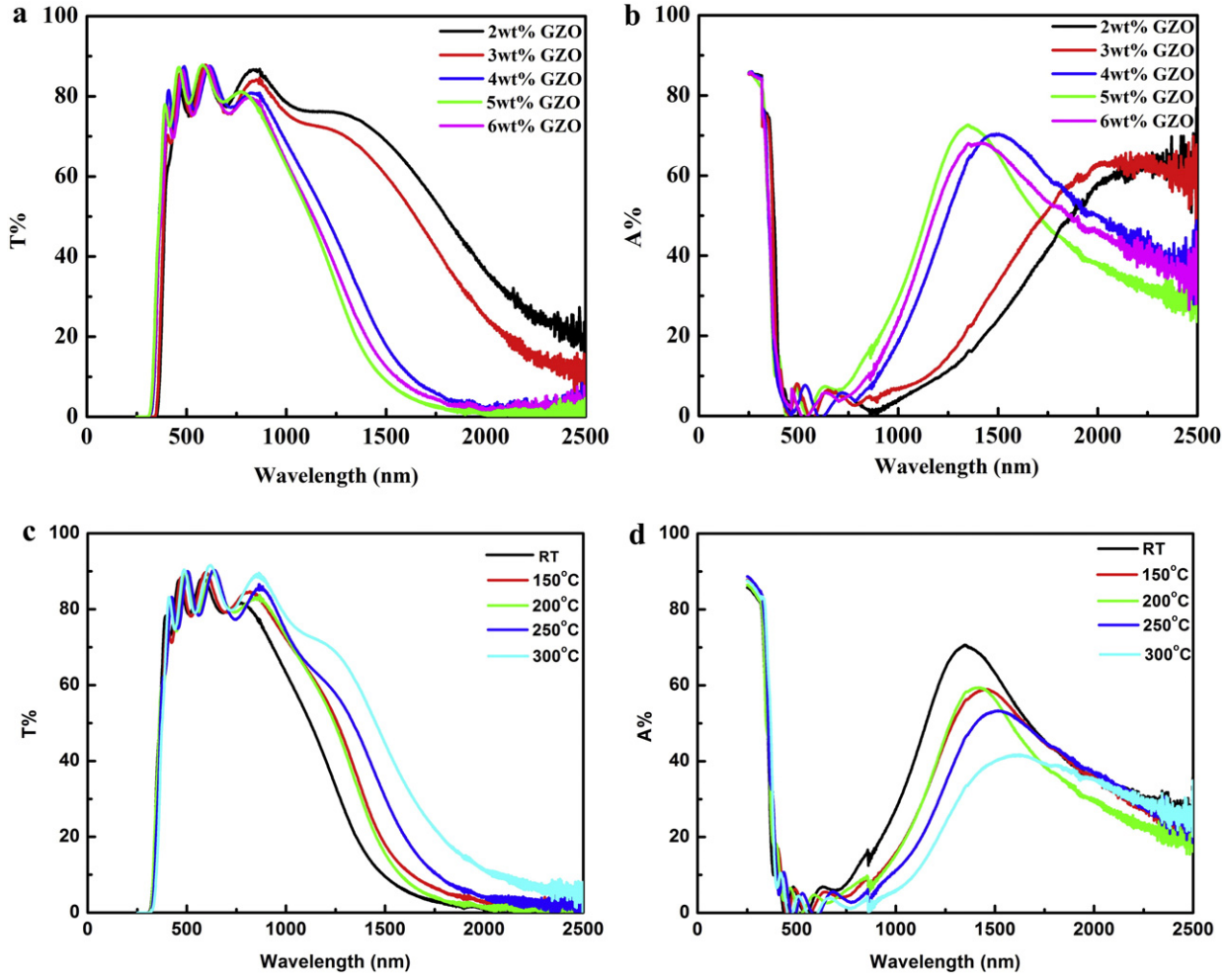

Fig. 4. Optical transmittance and optical absorption of GZO films grown (a), (b) at RT using the sputtering targets with various Ga_2O_3 doping contents (2, 3, 4, 5 and 6 wt%), and (c), (d) at various substrate temperatures (RT, 150, 200, 250 and 300 °C) using the sputtering target with a Ga_2O_3 doping content of 5 wt%.

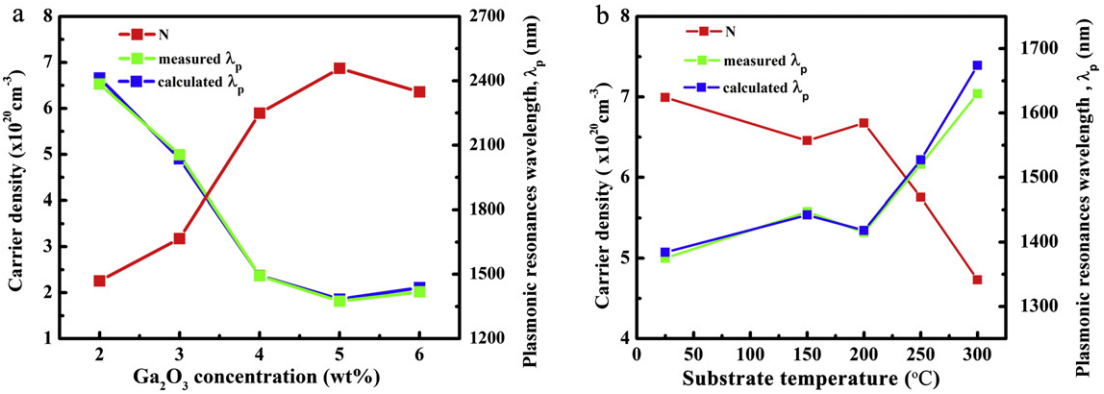

Fig. 5. Carrier concentration (n) and the plasma wavelength (λ_p) for GZO thin films grown (a) at RT using the sputtering targets with various Ga_2O_3 doping contents (2, 3, 4, 5 and 6 wt%), and (b) at various substrate temperatures (RT, 150, 200, 250 and 300 °C) using the sputtering target with a Ga_2O_3 doping content of 5 wt%.

where ε_∞ is the background permittivity, ω_p is the plasma frequency, Γ_p is the carrier relaxation rate, and f_l is the strength of the Lorentz oscillator with center frequency ω_l and damping Γ_l. The Lorentz oscillator model is suitable for ultraviolet band. The Drude model is suitable for visible and near-infrared wave band.

Fig. 6 shows the SE parameters Δ and Ψ of a GZO thin film (ceramic target with 5 wt% Ga_2O_3, deposited at room temperature) on glass measured for angle of incidence (AOI = 75°). Red line shows fit to the data using a model for the dielectric function of the GZO thin film. The mean square error is MSE ~ 6.1 for a fit over the whole wavelength range.

Fig. 7a and c shows the real parts of the permittivity of the GZO films as a function of Ng and Ts. The zero-cross-over of the real permittivity (defined as the wavelength at which the real part of the permittivity (ε_1) crosses zero) is observed to shift toward shorter wavelength due to the increased carrier concentration as Ng increases and Ts decreases respectively. The negative real permittivity at 1.55 μm guarantees Drude metal-like optical properties at telecommunication wavelengths, which is a necessary condition to be used as building blocks in the field of plasmonic metamaterial devices [47]. However, increasing the carrier concentration also leads to increased losses at the NIR range [11]. To compare the absorption of GZO films with metal materials, the ratios n/k with n and k being the real and imaginary parts of the refractive index of the GZO films deposited at different Ng and Ts are plotted in Fig. 7b and d. The larger ratio of n/k corresponds to less material absorption losses [48]. Although the absorption losses of GZO film increase as carrier concentration increases, the lowest ratio of all samples is also ten times larger than silver at the telecommunication wavelengths of 1.55 μm (Fig. 7b and d). Thus, the value of carrier concentration in GZO thin film is the dominating factor that determines the film from reaching the ideal.

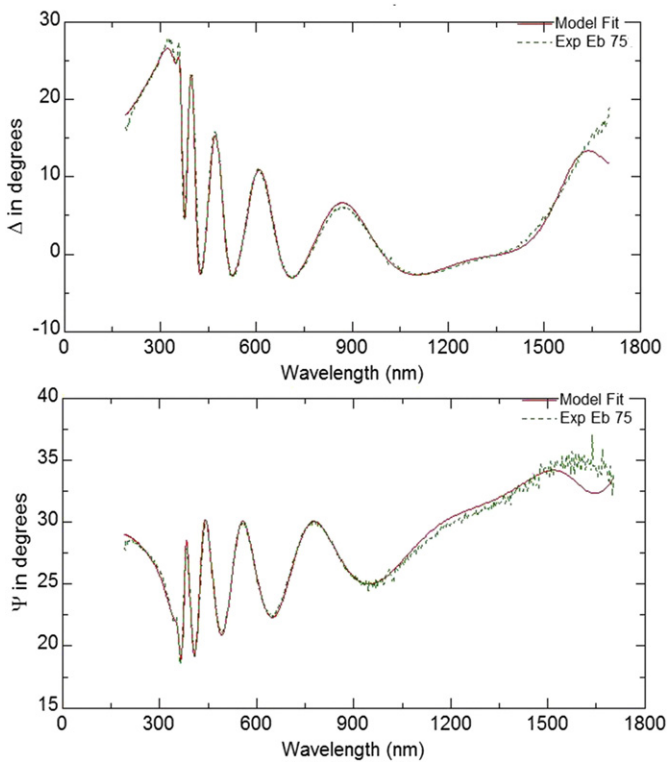

Fig. 6. Spectroscopic ellipsometric parameters Δ and Ψ of a GZO thin film (ceramic target with 5 wt% Ga_2O_3, deposited at room temperature) on glass measured for angle of incidence (AOI = 75°).

Fig. 8 shows the influences of target concentration and substrate temperature on tuning the GZO properties. There are three groups of histogram in Fig. 8. The first group represents the ratio of the adjustable extent of carrier concentration stem from varied target Ga_2O_3 concentration to that stem from varied temperature. The second group represents the ratio of the adjustable extent of plasmonic resonances wavelength stem from varied target Ga_2O_3 concentration to that stem from varied temperature. The third group represents the ratio of the adjustable extent of material absorption losses at 1.55 μm stem from varied target Ga_2O_3 concentration to that stem from varied temperature. The front column represents the ratio from target Ga_2O_3 concentration in each group. The later column represents the ratio from temperature in each group. Obviously, target Ga_2O_3 concentration has the most dominating influence on tuning the GZO properties.

4. Conclusions

In summary, the effects of Ga_2O_3 content in the target and substrate temperature on the electrical, structural and optical properties of GZO films deposited on glass substrates by RF magnetron sputtering are investigated. The Ng and Ts during deposition of these films have been optimized to achieve the highest possible carrier concentration and mobility. Enhancing the Ng increased the carrier concentration due to the increased number of substitution Ga. It is found that the film deposited at optimized conditions (Ng = 5 wt%, Ts = RT) has the highest carrier concentration of 7.0×10^{20} cm^{-3}. Correspondingly, the real part of the permittivity of the GZO film is negative at 1.55 μm, which is a necessary condition to be an ideal plasmonic metamaterials. In addition, the values of plasmonic resonances wavelength can be changed from 1.35 to 2.39 μm by adjusting the carrier concentration. Absorption

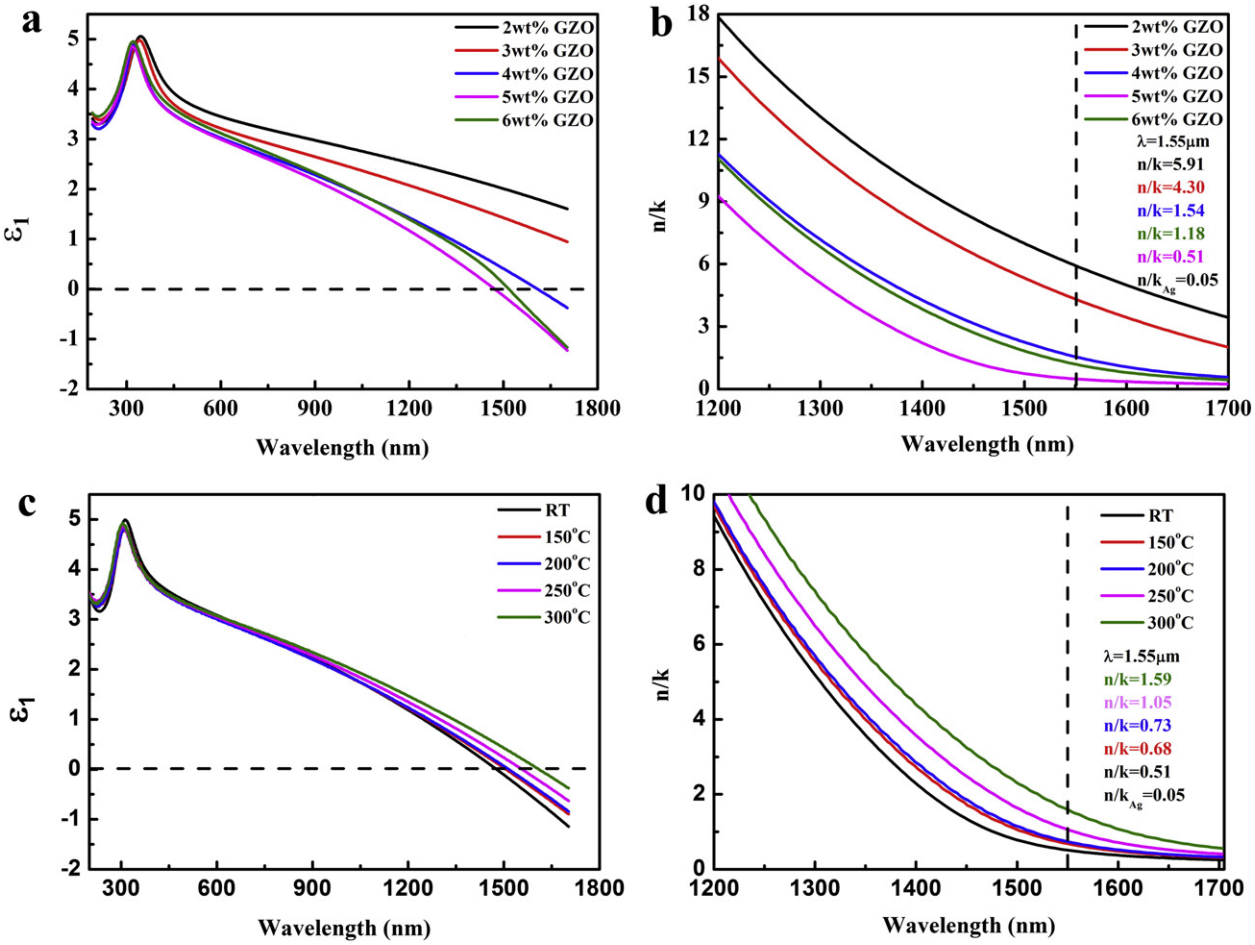

Fig. 7. Real parts of permittivity and the ratios n/k with n and k being the real and imaginary parts of the refractive index of the GZO film deposited (a), (b) at RT using the sputtering targets with various Ga_2O_3 doping contents (2, 3, 4, 5 and 6 wt%), and (c), (d) at various substrate temperatures (RT, 150, 200, 250 and 300 °C) using the sputtering target with a Ga_2O_3 doping content of 5 wt%.

losses in these GZO films are less 10 times smaller than those observed in conventional Ag films at the telecommunication wavelengths of 1.55 μm. These results show that the value of carrier concentration is the dominating factor that affected GZO films become a promising low-loss alternative material to conventional metals for plasmonic application at telecommunication wavelength.

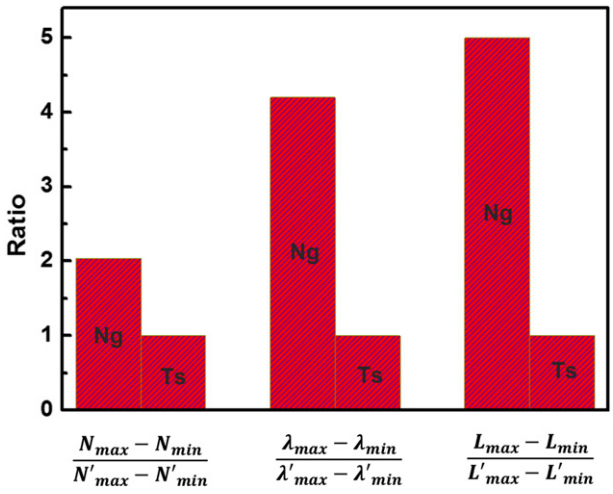

Fig. 8. The ratios of the adjustable extent of the GZO properties from target Ga_2O_3 concentration to that from temperature.

Acknowledgements

This work was supported by the National Natural Science Foundation of China (61275114, 21377063), the Ningbo Natural Science Foundation (Grant no. 2014A610039), the Ningbo Municipal Science and Technology Innovative Research Team (Grant No. 2015B11002) and the National Basic Research Program of China (2012CB934300 and 2011CBA00900).

Appendix A. Supplementary data

Supplementary data to this article can be found online at http://dx.doi.org/10.1016/j.tsf.2015.11.005.

References

[1] E. Ozbay, Plasmonics: merging photonics and electronics at nanoscale dimensions, Science 311 (2006) 189–193.
[2] G.A. Wurtz, R. Pollard, W. Hendren, G.P. Wiederrecht, D.J. Gosztola, V.A. Podolskiy, A.V. Zayats, Designed ultrafast optical nonlinearity in a plasmonic nanorod metamaterial enhanced by nonlocality, Nat. Nanotechnol. 6 (2011) 107–111.
[3] S. Xiao, V.P. Drachev, A.V. Kildishev, X. Ni, U.K. Chettiar, H.K. Yuan, V.M. Shalaev, Loss-free and active optical negative-index metamaterials, Nature 466 (2010) 735–738.
[4] N. Engheta, Circuits with light at nanoscales: optical nanocircuits inspired by metamaterials, Science 317 (2007) 1698–1702.
[5] M.L. Brongersma, R. Zia, J.A. Schuller, Plasmonics—the missing link between nanoelectronics and microphotonics, Appl. Phys. A Mater. Sci. Process. 89 (2007) 221–223.
[6] S. Lal, S. Link, N.J. Halas, Nano-optics from sensing to waveguiding, Nat. Photonics 1 (2007) 641–648.

[7] S.A. Maier, P.E. Barclay, T.J. Johnson, M.D. Friedman, O. Painter, Low-loss fiber accessible plasmon waveguide for planar energy guiding and sensing, Appl. Phys. Lett. 84 (2004) 3990–3992.
[8] D.C. Look, K.D. Leedy, ZnO plasmonics for telecommunications, Appl. Phys. Lett. 102 (2013) 182107.
[9] J. Homola, S.S. Yee, G. Gauglitz, Surface plasmon resonance sensors: review, Sensors Actuators B Chem. 54 (1999) 3–15.
[10] J.M. Luther, P.K. Jain, T. Ewers, A.P. Alivisatos, Localized surface plasmon resonances arising from free carriers in doped quantum dots, Nat. Mater. 10 (2011) 361–366.
[11] G.V. Naik, V.M. Shalaev, A. Boltasseva, Alternative plasmonic materials: beyond gold and silver, Adv. Mater. 25 (2013) 3264–3294.
[12] E.G. Maksimov, I.I. Mazin, S.N. Rashkeev, Y.A. Uspenski, First-principles calculations of the optical properties of metals, J. Phys. F: Met. Phys. 18 (1988) 833–849.
[13] C.J. Powell, The origin of the characteristic electron energy losses in ten elements, Proc. Phys. Soc. 76 (1960) 593–610.
[14] M.A. Noginov, L. Gu, J. Livenere, G. Zhu, A.K. Pradhan, R. Mundle, M. Bahoura, Y.A. Barnakov, V.A. Podolskiy, Transparent conductive oxides: plasmonic materials for telecom wavelengths, Appl. Phys. Lett. 99 (2011) 021101.
[15] A. Calzolari, A. Ruini, A. Catellani, Transparent conductive oxides as near-IR plasmonic materials: the case of Al-Doped ZnO derivatives, ACS Photonics 1 (2014) 703–709.
[16] P.R. West, S. Ishii, G.V. Naik, N.K. Emani, V.M. Shalaev, A. Boltasseva, Searching for better plasmonic materials, Laser Photonics Rev. 4 (2010) 795–808.
[17] A. Boltasseva, H.A. Atwater, Low-loss plasmonic metamaterials, Science 331 (2011) 290–291.
[18] G.V. Naik, J. Kim, A. Boltasseva, Oxides and nitrides as alternative plasmonic materials in the optical range [Invited], Opt. Mater. Express 1 (2011) 1090–1099.
[19] H.J. Ko, Y.F. Chen, S.K. Hong, H. Wenisch, T. Yao, D.C. Look, Ga-doped ZnO films grown on GaN templates by plasma-assisted molecular-beam epitaxy, Appl. Phys. Lett. 77 (2000) 3761–3763.
[20] T. Yim, C. Lee, Dependence of the electrical and optical properties of sputter-deposited ZnO:Ga films on the annealing temperature, time, and atmosphere, J. Mater. Sci. Mater. Electron. 18 (2007) 385–390.
[21] F. Wu, L. Fang, Y.J. Pan, K. Zhou, Q.L. Huang, C.Y. Kong, Effect of substrate temperature on the structural, electrical and optical properties of ZnO: Ga thin films prepared by RF magnetron sputtering, Phys. E. 43 (2010) 228–234.
[22] H. Kim, M. Osofsky, S.M. Prokes, O.J. Glembocki, A. Piqué, Optimization of Al-doped ZnO films for low loss plasmonic materials at telecommunication wavelengths, Appl. Phys. Lett. 102 (2013) 171103.
[23] S. Kalusniak, S. Sadofev, P. Schäfer, F. Henneberger, Heavily n-type ZnO: a plasmonic material at telecommunication wavelengths, Phys. Status Solidi C 11 (2014) 1357–1360.
[24] S.D. Shinde, A.V. Deshmukh, S.K. Date, V.G. Sathe, K.P. Adhi, Effect of Ga doping on micro/structural, electrical and optical properties of pulsed laser deposited ZnO thin films, Thin Solid Films 520 (2011) 1212–1217.
[25] T. Terasako, Y. Ogura, S. Fujimoto, H. Song, H. Makino, M. Yagi, S. Shirakata, T. Yamamoto, Carrier transport and photoluminescence properties of Ga-doped ZnO films grown by ion-plating and by atmospheric-pressure CVD, Thin Solid Films 549 (2013) 12–17.
[26] N. Taewook, C.W. Lee, H.J. Kima, H. Kima, Growth characteristics and properties of Ga-doped ZnO (GZO) thin films grown by thermal and plasma-enhanced atomic layer deposition, Appl. Surf. Sci. 295 (2014) 260–265.
[27] R. Prabakaran, T. Monteiro, M. Peres, A.S. Viana, A.F. da Cunha, H. Águas, A. Gonçalves, E. Fortunato, R. Martins, I. Ferreira, Optical and structural analysis of porous silicon coated with GZO films using rf magnetron sputtering, Thin Solid Films 515 (2007) 8664–8669.
[28] V. Assuncao, E. Fortunato, A. Marquesa, H. Águas, I. Ferreira, M.E.V. Costa, R. Martins, Influence of the deposition pressure on the properties of transparent and conductive ZnO: Ga thin-film produced by rf sputtering at room temperature, Thin Solid Films 427 (2003) 401–405.
[29] W.J. Cho, Y.H. Joung, S.J. Kang, Effect of Ga doping concentrations, substrate temperatures and working pressures on the electrical and optical properties of ZnO thin films, J. Mater. Sci. Mater. Electron. 25 (2014) 3901–3906.
[30] S.M. Park, T. Ikegami, K. Ebihara, Effects of substrate temperature on the properties of Ga-doped ZnO by pulsed laser deposition, Thin Solid Films 513 (2006) 90–94.
[31] T. Yamamoto, T. Sakemi, K. Awai, S. Shirakata, Dependence of carrier concentrations on oxygen pressure for Ga-doped ZnO prepared by ion plating method, Thin Solid Films 451 (2004) 439–442.
[32] G.S. Arnold, Absorptivity of several metals at 10.6 μm: empirical expressions for the temperature dependence computed from Drude theory, Appl. Opt. 23 (1984) 1434–1436.
[33] T. Matsumoto, K. Mizuguchi, T. Horii, S. Sano, T. Muranaka, Y. Nabetani, S. Hiraki, H. Furukawa, A. Fukasawa, S. Sakamoto, S. Hagihara, H. Kono, K. Kijima, O. Abe, K. Yashiro, Effects of Ga doping and substrate temperature on electrical properties of ZnO transparent conducting films grown by plasma-assisted deposition, Jpn. J. Appl. Phys. 50 (2011) 05FB13.
[34] Q. Ma, Z. Ye, H. He, L. Zhu, W. Liu, Y. Yang, L. Gong, J. Huang, Y. Zhang, B. Zhao, Highly near-infrared reflecting and transparent conducting ZnO:Ga films: substrate temperature effect, J. Phys. D. Appl. Phys. 41 (2008) 055302.
[35] J. Kim, G.V. Naik, N.K. Emani, A. Boltasseva, Plasmonic resonances in nanostructured transparent conducting oxide films, IEEE J. Sel. Top. Quantum 19 (2013) 4601907.
[36] C. Zhu, J. Li, Y. Yang, J. Huang, Y. Lu, R. Tan, N. Dai, W. Song, Zn-aided defect control for ultrathin GZO films with high carrier concentration aiming at alternative plasmonic metamaterials, Phys. Status Solidi A 212 (2015) 1713–1718.
[37] K.J. Ahn, J.H. Park, B.K. Shin, W. Lee, G.Y. Yeom, J.M. Myoung, Effect of sputtering power on the properties of ZnO: Ga transparent conductive oxide films deposited by pulsed DC magnetron sputtering with a rotating cylindrical target, Appl. Surf. Sci. 271 (2013) 216–222.
[38] Y.H. Kim, J. Jeong, K.S. Lee, B. Cheong, T.Y. Seong, W.M. Kim, Effect of composition and deposition temperature on the characteristics of Ga doped ZnO thin films, Appl. Surf. Sci. 257 (2010) 109–115.
[39] D.H. Lee, K. Kim, Y.S. Chun, S. Kim, S.Y. Lee, Substitution mechanism of Ga for Zn site depending on deposition temperature for transparent conducting oxides, Curr. Appl. Phys. 12 (2012) 1586–1590.
[40] Q.B. Ma, Z.Z. Ye, H.P. He, J.R. Wang, L.P. Zhu, B.H. Zhao, Structural, electrical, and optical properties of transparent conductive ZnO: Ga films prepared by DC reactive magnetron sputtering, J. Cryst. Growth 304 (2007) 64–68.
[41] J.T. Thienprasert, S. Rujirawat, W. Klysubun, J.N. Duenow, T.J. Coutts, S.B. Zhang, D.C. Look, S. Limpijumnong, Compensation in Al-doped ZnO by Al-related acceptor complexes: synchrotron X-ray absorption spectroscopy and theory, Phys. Rev. Lett. 110 (2013) 055502.
[42] C.W. Gorrie, A.K. Sigdel, J.J. Berry, B.J. Reese, M.F.A.M. van Hest, P.H. Holloway, D.S. Ginley, J.D. Perkins, Effect of deposition distance and temperature on electrical, optical and structural properties of radio-frequency magnetron-sputtered gallium-doped zinc oxide, Thin Solid Films 519 (2010) 190–196.
[43] T. Minami, H. Sato, H. Nanto, S. Takata, Group III impurity doped zinc oxide thin films prepared by RF magnetron sputtering, Jpn. J. Appl. Phys. 24 (1985) L781–L784.
[44] A.L. Patterson, The Scherrer formula for X-ray particle size determination, Phys. Rev. 56 (1939) 978–982.
[45] H.T. Cao, C. Sun, Z.L. Pei, A.Y. Wang, L.S. Wen, R.J. Hong, X. Jiang, Properties of transparent conducting ZnO: Al oxide thin films and their application for molecular organic light-emitting diodes, J. Mater. Sci. Mater. Electron. 15 (2004) 169–174.
[46] T.J. Coutts, D.L. Young, T.A. Gessert, Modeling, characterization, and properties of transparent conducting oxides, in: D.S. Ginley, H. Hosono, D.C. Paine (Eds.), Handbook of Transparent Conductors, Springer, US 2011, pp. 51–100.
[47] J. Kim, G.V. Naik, A.V. Gavrilenko, K. Dondapati, V.I. Gavrilenko, S.M. Prokes, O.J. Glembocki, V.M. Shalaev, A. Boltasseva, Optical properties of gallium-doped zinc oxide—a low-loss plasmonic material: first-principles theory and experiment, Phys. Rev. X 3 (2013) 041037.
[48] S.C. Kehr, Y.M. Liu, L.W. Martin, P. Yu, M. Gajek, S.Y. Yang, C.H. Yang, M.T. Wenzel, R. Jacob, H.G. von Ribbeck, M. Helm, X. Zhang, L.M. Eng, R. Ramesh, Near-field examination of perovskite-based superlenses and superlens-enhanced probe-object coupling, Nat. Commun. 2 (2011) 249.